Numerical Simulations of the Flow Around a Circular Cylinder Covered by a Porous Medium

Michal P. Sobera [1, 2], Chris R. Kleijn [1]
Harry E. A. van den Akker [1] and Paul Brasser [2]
[1] Kramers Laboratorium voor Fysische Technologie, TU Delft, Prins Bernhardlaan 6
2628 BW Delft, The Netherlands, Tel. +31 15 2781400, Fax. +31 15 2782838
[2] TNO Prins Maurits Laboratory, P.O. Box 45 2280 AA Rijswijk, The Netherlands
Tel. +31 15 284 3506, Fax. +31 15 284 3303

SUMMARY

In order to develop more comfortable and safe protective garments, it is necessary to obtain detailed knowledge of the phenomena governing air flow, heat and mass transfer. Computational Fluid Dynamics (CFD) is a promising approach for those kinds of problems. Numerical simulations can support the design process and make it cheaper. Simulations of the air flow in a 2D model of a cylindrical human body part covered by protective clothing are presented here. The CFD predictions show dependencies of the air flow penetrating the clothing material, and the heat and mass transfer to the body part, as a function of external flow and clothing material properties. The problem has been formulated by using dimensionless parameters, reducing the number of properties for flow and clothing conditions. The clothing material has been modeled as a porous material. For turbulence modeling, we used an RNG k-ε model. The set of governing differential equations has been solved numerically by use of the commercial flow-simulation code Fluent 5.

INTRODUCTION

Investigation of the phenomena which play a dominant role in processes of heat and mass transfer in protective clothing systems, is still a big challenge for researchers. The problems can be analyzed through theoretical models, experimental studies and numerical simulations. During last years, computer power has increased significantly, allowing for the numerical simulation of increasingly complex applications. In this paper, we apply **C**omputational **F**luid **D**ynamics to protective clothing modeling. Numerical studies were performed for better understanding of air penetration through the clothing – body part system.

We considered a 2-dimensional cylindrical body, covered by a porous medium, placed in a uniform turbulent air flow. This is the simplest model of human body part (e.g. an arm) covered by a protective clothing. Figure 1 shows schematically the problem formulation. We have considered the body part as a solid cylinder, and protective garment as a porous layer, characterized by a given air permeability. The space between the clothing material and the body part is filled with air. We considered steady state flow situations only (no changes of mean flow properties in the time, no movement of the body part).

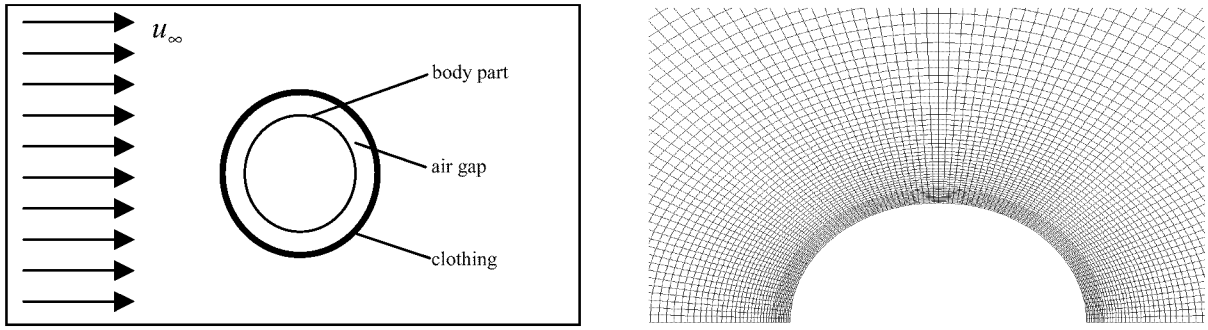

Figure 1. *Schematic problem formulation (a) and a small part of computational domain with mesh (b)*

Paper presented at the RTO HFM Symposium on "Blowing Hot and Cold: Protecting Against Climatic Extremes", held in Dresden, Germany, 8-10 October 2001, and published in RTO-MP-076.

NOMENCLATURE

Roman letters

c	mass fraction
c_p	specific heat, J/kg/K
Da	Darcy number, see Table 1
Da_s	Damköhler number, see Table 1
D	diffusivity, m^2/s
I_c	porous thickness ratio
I_g	air gap thickness ratio
K	permeability of the porous medium, m^2
L	characteristic length
Nu	Nusselt number, see Table 1
Pr	Prandtl number, see Table 1
P	pressure, Pa
Re	Reynolds number, see Table 1
Sc	Schmidt number, see Table 1
Sh	Sherwood number, see Table 1
$\boldsymbol{S}$	source term vector, Pa/m
T	temperature, °C
u_∞	free stream velocity, m/s
$\overline{V}$	mean velocity component, m/s
v'	fluctuating velocity component, m/s
$\boldsymbol{V}$	velocity vector, m/s

Greek letters

α	binary parameter
δ_c	porous medium thickness, m
δ_g	air gap thickness, m
λ	thermal conductivity, W/mK
μ	viscosity, Pa·s
ρ	density, kg/m^3

Subscript

∞	free stream
c	cloth
g	air gap

COMPUTATIONAL DETAILS

The fluid flow around blunt bodies is described by a set of differential equations: the continuity equation and the *Navier-Stokes* or momentum balance equation [7]. In general the mass conservation (continuity) equation is given by formula:

$$\frac{\partial \rho}{\partial t} + \nabla \cdot (\rho \boldsymbol{V}) = 0 \tag{1}$$

for steady state ($\partial/\partial t = 0$) and incompressible flow ($\rho = const.$) we can write:

$$\nabla \cdot \boldsymbol{V} = 0 \tag{2}$$

The momentum equation for steady state and incompressible flow is given by:

$$\rho \nabla \cdot (\boldsymbol{V}\boldsymbol{V}) = -\nabla P + \nabla \cdot \overline{\overline{\tau}} + \alpha \boldsymbol{S} \tag{3}$$

where α is a binary parameter:

$$\alpha = \begin{cases} 1 & \text{in the porous region} \\ 0 & \text{in the fluid region} \end{cases}$$

$\overline{\overline{\tau}}$ denotes the viscous stresses tensor, given by:

$$\overline{\overline{\tau}} = \mu \left(\nabla \boldsymbol{V} + (\nabla \boldsymbol{V})^T \right) \tag{4}$$

and $(\cdot)^T$ denotes a transposed vector. The momentum source term in the porous region is equal to the pressure gradient in the porous medium in accordance to the Darcy equation:

$$\boldsymbol{S} = \frac{\mu}{K} \boldsymbol{V} . \tag{5}$$

The heat transfer equation for the considered system may be written as:

$$\rho c_p (\boldsymbol{V} \nabla) T = \lambda \nabla^2 T \tag{6}$$

and in a similar way the species transport equation for a gas that is present in the air in small concentrations

$$(\boldsymbol{V} \nabla) c = D \nabla^2 c \,. \tag{7}$$

Here it is assumed, that heat and mass transfer through the clothing is mainly convective, and solid heat conduction and mass diffusion in the clothing fiber material is neglected.

The above equations have been presented in dimensional form. In order to reduce the number of parameters describing the problem, it is more useful to make the equations dimensionless by scaling the variables with a reference value. As a result, dimensionless parameters appear in the equations, describing the problem has been presented (see Table 1).

Dimensionless group	**Definition**
Reynolds number (Re)	$\frac{\rho u_\infty L}{\mu}$
Darcy number (Da)	$\frac{K}{\delta_c^2}$
Damköhler number (Da_s)	$\frac{k_r \delta_g}{D}$
Prandtl number (Pr)	$\frac{\mu c_p}{\lambda}$
Schmidt number (Sc)	$\frac{\mu}{\rho D}$
porous thickness ratio (I_c)	$\frac{\delta_c}{L}$
air gap thickness ratio (I_g)	$\frac{\delta_g}{L}$

Table 1. *The set of dimensionless parameters used for describing the discussed problem*

Assuming constant air properties, we can make above equations dimensionless by introducing the following dimensionless parameters:

$$\hat{\boldsymbol{V}} = \frac{\boldsymbol{V}}{u_\infty} \qquad \hat{c} = \frac{c}{c_\infty} \qquad \hat{T} = \frac{T - T_\infty}{T_S - T_\infty} \qquad \hat{P} = \frac{P}{\rho_{ref} u_\infty^2} \qquad \hat{\nabla} = \nabla L \tag{8}$$

where u_∞ is the free stream velocity, c_∞ is the free stream concentration of the trace gas, T_∞ is the free stream air temperature, T_s is the surface temperature of the inner cylinder, and L is the characteristic length taken here as the outer cylinder diameter. This leads to dimensionless equations as below:

1. Continuity equation:

$$\nabla \cdot \hat{\boldsymbol{V}} = 0 \tag{9}$$

2. Momentum equation:

$$\nabla \cdot \left(\hat{\boldsymbol{V}} \hat{\boldsymbol{V}}\right) = -\hat{\nabla} \hat{P} + \frac{1}{Re} \hat{\nabla} \cdot \left[\hat{\nabla} \hat{\boldsymbol{V}} + \left(\hat{\nabla} \hat{\boldsymbol{V}}\right)^T\right] + \alpha \frac{I_c^2}{Da\, Re} \hat{\boldsymbol{V}} \tag{10}$$

3. Heat transfer equation:

$$\left(\hat{\boldsymbol{V}} \hat{\nabla}\right) \hat{T} = -\frac{1}{Re\, Pr} \hat{\nabla}^2 \hat{T} \tag{11}$$

4. Species transport equation:

$$\left(\hat{\boldsymbol{V}} \hat{\nabla}\right) \hat{c} = -\frac{1}{Re\, Sc} \hat{\nabla}^2 \hat{c} \tag{12}$$

The computational domain consists of three parts: the external air flow, the porous medium and the air gap between the body part and porous cylinder. The outer flow has been considered as a turbulent. The porous medium has been treated by adding a momentum sink, in accordance with Darcy's law, to the momentum equation (10). The flow in the air gap has been treated as laminar because the highest value of Reynolds number based on air gap width was $5 \cdot 10^2$.

For the outer, turbulent flow, we used **RANS** ("*Reynolds Averaged" Navier-Sokes*) approach to obtain turbulence correlations that needs modeling. The instantaneous velocity vector is decomposed into a mean and a fluctuating component, viz.:

$$\boldsymbol{V} = \overline{\boldsymbol{V}} + \boldsymbol{v}' \tag{13}$$

where $\overline{\boldsymbol{V}}$ is the time averaged velocity and $\boldsymbol{v}'$ is the fluctuating component of the velocity [6]. By putting (13) into momentum equation (10), the RANS equations are obtained, which have similar general form as the instantaneous NS equation (10), with the velocity and pressure now representing time- or ensemble-averaged values. Additional terms now appear, representing turbulence effects. These so-called Reynolds stress terms have to be modeled in order to close the RANS equations. In order to model the Reynolds stresses, we used a two-equation model eddy viscosity model. Within this model, turbulence is modeled by replacing the molecular viscosity in the momentum equation by an eddy or turbulent viscosity, which is calculated from the turbulence kinetic energy (k) and turbulence dissipation rate (ε). Two additional transport equations are solved for k and ε [6].

A part of the used computational domain has been presented in Figure 1b. In order to safe computational time, we considered only the upper half of physical space (Figure 1a), based on the symmetry of the flow, using the symmetry boundary condition. In the inlet at the left hand side of the domain, a uniform horizontal velocity was specified, as well as a uniform inlet temperature and species concentration. On the surface of the inner cylinder, a no-slip boundary condition was prescribed for the velocity, as well as a uniform surface temperature. Furthermore, it was assumed that the trace gas species in the air deposits on the inner cylinder wall through a first order deposition reaction with rate $R=k_r c$. For $k_r \to 0$, this corresponds to a zero-flux Neuman boundary condition on the cylinder wall, whereas for $k_r \to \infty$, it corresponds to a $c = 0$ Dirichlet boundary condition. The other boundaries of the domain were defined as free outlets. The boundary conditions in the inlet and on the cylinder wall are listed below:

1. Inlet boundary conditions:

$$\begin{aligned} V_x &= u_\infty \quad \to \quad \hat{V}_x = 1 \\ V_y &= 0 \quad \to \quad \hat{V}_y = 0 \\ \boldsymbol{v}' &= \frac{u_\infty}{20} \quad \to \quad \hat{\boldsymbol{v}}' = 0.05 \\ T &= T_\infty \quad \to \quad \hat{T} = 0 \\ c &= c_\infty \quad \to \quad \hat{c} = 1 \end{aligned} \tag{14}$$

2. Boundary conditions at the surface of the inner cylinder:

$$\begin{aligned} \boldsymbol{V} &= 0 \quad \to \quad \hat{\boldsymbol{V}} = 0 \\ T &= T_s \quad \to \quad \hat{T} = 1 \\ D\frac{\partial c}{dn} &= k_r c \quad \to \quad \frac{\partial \hat{c}}{d\hat{n}} = \frac{Da_s}{I_g} \end{aligned} \tag{15}$$

Two-dimensional computations were performed using the Fluent 5, based on the well-known pressure correction SIMPLE algorithm [3] and finite volume formulation. Second order differencing scheme has been used for all equations. As mentioned previously, two-equation turbulence model (known as k-ε) has been employed. Because of the known weakness of the standard k-ε model for cases such as the one considered here [4], the *RNG* version of k-ε has been used [5], which is known to perform better for flow around bluff bodies. The computations were performed with a standard desktop PC configuration (Intel PIII 800MHz, 192 Mb RAM).

RESULTS AND DISCUSSION

Aerodynamics results

First, the aerodynamics of the studied system has been considered. The goal of this part of the work was to study flow dependencies on the Reynolds and Darcy number. A standard case has been defined, with $Re = 7 \cdot 10^3$ and $Da = 6.6 \cdot 10^{-4}$ (for an 8 cm diameter inner cylinder and a cloth thickness of 0.5 mm, this corresponds to a free air velocity $u_\infty = 1.3$ m/s, and a cloth permeability $K = 0.16 \cdot 10^{-9}$ m^2, the latter leads to an air resistance of 15 Pa/(m/s)). In all cases I_c was $5 \cdot 10^{-3}$, I_c was $5 \cdot 10^{-2}$, Pr was 0.7 and Sc was 1.2. All of the described cases were in the subcritical flow regime, the highest Reynolds number being $Re = 35 \cdot 10^3$ [1].

Figure 2a presents the streamline distribution for the standard case. Analyzing this graph we can distinguish two regions in the air gap between the body part and the clothing material: The upstream region, where air flows through the clothing into the air gap, and a second region, where air flows out again. In order to see where the border between these two regions is, we can analyze Figure 2b. This graph presents the pressure coefficient distribution for the surface of the outer and inner cylinder, as a function of the angle Θ, measured from the upstream stagnation point. From $\Theta = 0°$ up to about $\Theta = 52°$, the pressure outside the clothing is higher than inside. This is the region where air flows through the clothing into the air gap. For $\Theta > 52°$, the pressure outside is lower than pressure inside the air gap, and air flows out. The outer pressure distribution is almost identical to known results for a single solid cylinder, as reported by different investigators in experimental work [2]. The shape of outer pressure distribution curve also proofs the subcritical character of the flow [1], [9].

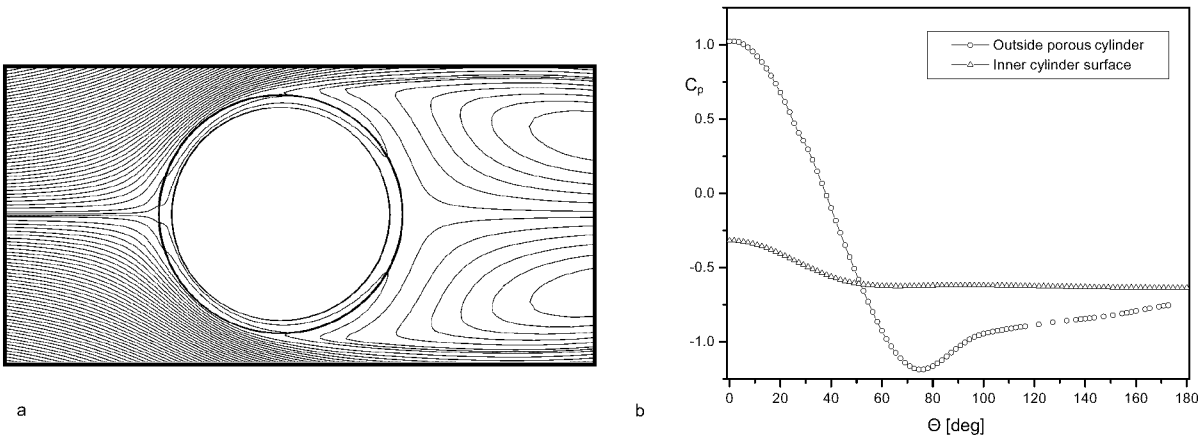

Figure 2. *Stream lines (a) and pressure coefficient distribution (b) for typical case*

Figures 3a and 3b present the tangential velocity component inside the air gap, averaged across the air gap height, as a function of angle. For the ease of comparison, the computed velocities have been normalized with free stream velocity.

In Figure 3a, normalized averaged tangential velocities have been displayed for different values of Darcy number and a fixed Reynolds number $Re = 7 \cdot 10^3$. For higher value of Darcy number, and consequently for higher permeability, the normalized air velocities inside the air gap are higher. The normalized velocity depends approximately linear on the Darcy number.

Figure 3b presents the normalized averaged tangential velocity component for fixed Darcy number $Da = 6.6 \cdot 10^{-4}$ and different values of the Reynolds number. For higher value of the Reynolds number, and consequently for higher air velocities, the normalized air velocities inside the air gap are higher. The dependence of the normalized velocity on the Reynolds number is again approximately linear.

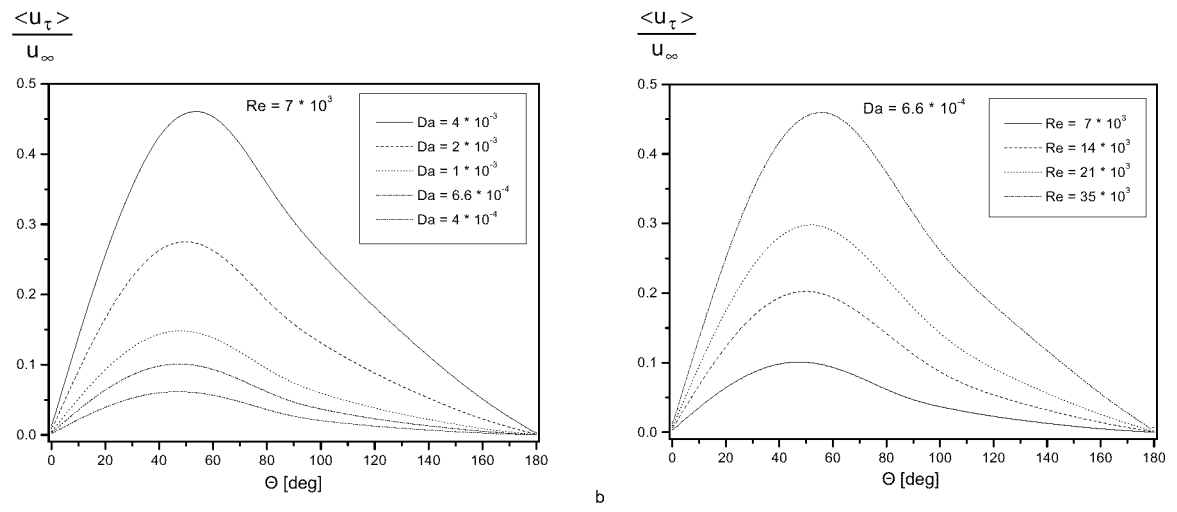

Figure 3. *Averaged tangential velocity component inside air gap as a function of angle for different Darcy (a) and Reynolds (b) number*

The observed behavior, i.e. the similar dependence of the normalized velocities in the air gap on the Darcy and the Reynolds number, can be explained from their similar appearance in the momentum sink term in the Navier-Stokes equation (10):

$$\hat{S} = \frac{I_c^2}{Da\,Re}\hat{\mu}\hat{V} \tag{16}$$

For the considered problem we have: $\hat{\mu} = const$ and $I_c^2 = const$, which implies:

$$\hat{V} \sim Da\,Re\,. \tag{17}$$

It should be noticed, that the Reynolds number is based on the diameter of the outer cylinder, whereas the Darcy number is based on the porous material thickness.

Heat and mass transfer results

The heat transfer to the inner cylinder (body part) has been computed for three different values of the Darcy and Reynolds number. Results are presented in Figure 4a, b and c, each of which presents six different curves for given Reynolds number $Re = 7{\cdot}10^3$, $14{\cdot}10^3$ and $35{\cdot}10^3$, respectively. The first group of displayed quantities is the dimensionless air temperature $<T>$, averaged over the height of the air gap (left axis). The second group gives the distribution of the local Nusselt number Nu (right axis). Both of them are presented for three values of the Darcy number, $Da = 4{\cdot}10^{-4}$, $6.6{\cdot}10^{-4}$ and $10{\cdot}10^{-4}$, respectively.

For the lowest value of the Reynolds number, the temperature distribution has a maximum around $\Theta = 100 - 120°$. For higher Darcy number, the maximum becomes smoother and shifts to larger angles. In Figure 4b, at a higher Reynolds number, we can observe similar behavior, but the temperature distribution becomes smoother and the maximum is located at larger angles. Comparable results have been found in [8]. The last picture, at the highest Reynolds number, shows a bit different behavior: for the lowest value of Darcy we can observe a smooth shape of the temperature distribution, but no maximum is present. For the higher Darcy numbers, the temperature curve has again a maximum. It appears because the flow inside the air gap changes, exhibiting a separation point and a recirculation zone. For every graph we can notice that the most efficient cooling occurs at locations where outer air enters the air gap (see Figure 2a and b). Analyzing the local Nusselt number distribution in figures 4a, b and c, we can observe exactly the same dependencies on the Darcy and Reynolds number. The highest value of Nusselt number responds to the highest heat flux and in consequence to the most efficient cooling.

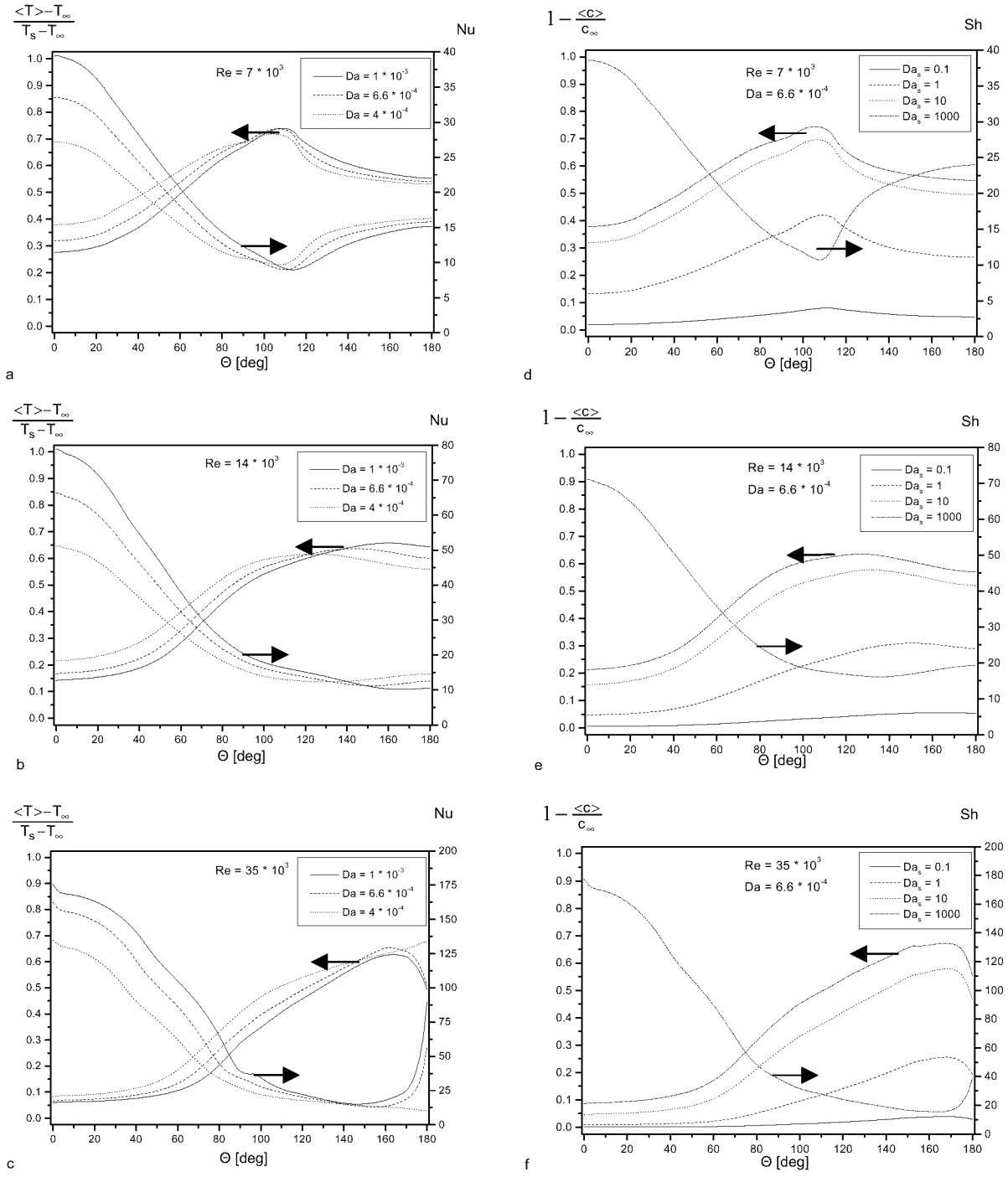

Figure 4. *Averaged relative temperature inside air gap and local Nusselt number (a, b, c) as a function of angle for different Darcy number and averaged relative mass fraction inside air gap and local Sherwood number (d, e, f) as a function of angle for different Damköhler number*

Mass transfer has been computed for the same three different Reynolds numbers, and a fixed Darcy number $Da = 6.6 \cdot 10^{-4}$. For these calculations, a trace gas (mass fraction 1%) was added to the air flow. It was assumed that the physical properties of the air and trace gas mixture were equal to those of air. On the surface of the inner cylinder, the trace gas is absorbed according to a first order reaction. The surface reaction rate is related to the Damköhler number. In Figure 4d, e and f, the dimensionless trace gas mass fraction profiles, again averaged over the height of the air gap, are presented for different surface reaction rate (left

axis). The lowest value of Damköhler number corresponds to the lowest surface reaction rate, meaning that most of the transported gas is not absorbed on the inner cylinder surface. It is easy to observe the influence of reaction rate on the mass fraction distribution. For low values of Damköhler number there is almost no difference between the free stream concentration and the concentration in the air gap between clothing and body part. When the reaction rate increases, the concentration inside the air gap becomes smaller than the free stream concentration, up to the extreme case when $Da_s \rightarrow \infty$ and the surface concentration is almost zero. The highest presented value of Damköhler number is $Da_s = 1000$, because the differences of averaged concentration profiles for higher Da_s are negligible. For large values of Da_s (corresponding to a Dirichlet boundary condition $c = 0$ at the inner cylinder surface), the dependency of the mass fraction distribution on the Reynolds number is very similar to the previously described dependency of the temperature distribution: for the lowest value of the Reynolds number, the concentration profile has a clear maximum. For the next higher Reynolds number (Figure 4e), the mass fraction curve has a smoother shape and the extreme value occurs at larger angle. At the highest Reynolds number, the influence of flow separation inside the air gap can again be observed. As is to be expected, for large values of Da_s, the Sherwood number for mass transfer to the inner cylinder is almost identical to the Nusselt number for heat transfer. Small differences being due to the fact that the Prandtl number for heat diffusion ($Pr = 0.7$) is not exactly equal to the Schmidt number for mass diffusion ($Sc = 1.2$).

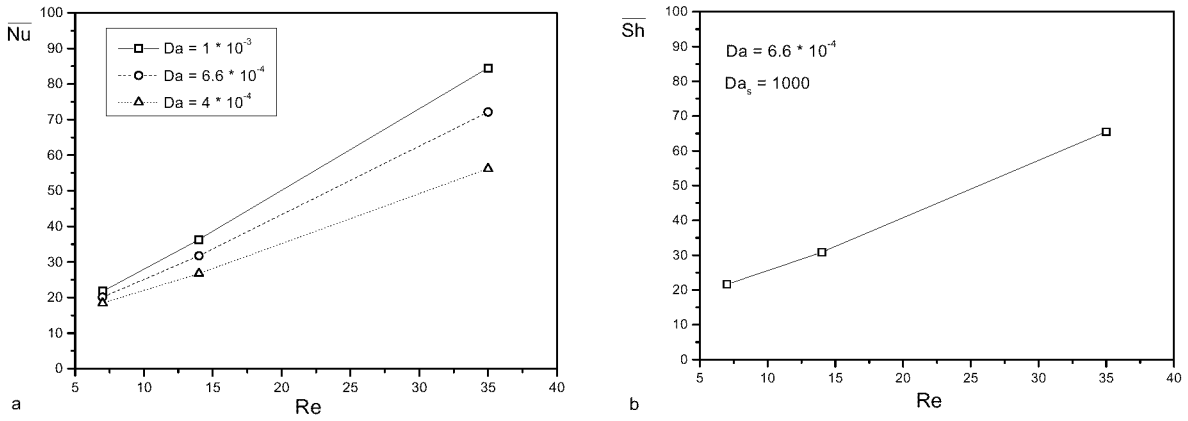

Figure 5. *Averaged Nusselt (a) and Sherwood number for large Damköhler number (b) as a function of Reynolds number*

Figure 5 presents the Nusselt and Sherwood number (for large Da_s), averaged over the entire surface of the inner cylinder, as a function of Reynolds number (based on the outer cylinder diameter). For the same value of the Darcy number, heat and mass transfer are almost identical, as expected. Surprising is the linear dependence of *Nu* and *Sh* on *Re*. This can be understood as follows: Based on well-know correlations for the heat transfer of a long cylinder, the Nusselt number can be written as

$$Nu \sim \left(\frac{< v_\tau > \delta_c \rho}{\mu} \right)^{\frac{1}{2}} \cdot Pr^{\frac{1}{3}} \tag{18}$$

From our analysis we found, that

$$\frac{< v_\tau >}{u_\infty} \sim Re \tag{19}$$

Combining these two equations, we find (for fixed ρ, μ and δ_c)

$$Nu \sim Re \cdot Pr^{\frac{1}{3}} . \tag{20}$$

A similar analysis can be given for the Sherwood number. This explains the linear dependence of the Nusselt and Sherwood number on the Reynolds number. For higher values of Reynolds, heat and mass transfer become more intensive.

CONCLUSIONS

In this paper, the dependency of air flow and heat and mass transfer through protective clothing around a cylindrical body part was studied as a function of the external flow velocity and the clothing material permeability. All results have been presented in dimensionless form, making them more generally applicable. One of the most important conclusions is that the air flow enters through the clothing material for angles up to $50-60°$ (measured from the stagnation point) only. This gives a general impression on locations, which are sufficiently ventilated, the others which are more endangered by poisonous gases in the air. The heat and mass transfer results accurately confirm the noticed effect; the lowest values of temperatures and highest for concentration appear for angles up to $50-60°$. For the same angle range, a maximal value of Nusselt and Sherwood numbers occurs, indicating large heat and mass transfer for this region.

REFERENCES

[1] – Celik, I., Shafer, F.D., 1995, "Long time-averaged solutions of turbulent flow past a circular cylinder", J. Wind Engineering and Industrial Aerodynamics, **56** pp. 185-212.

[2] – Kind, R.J., Jenkis, C. A., Broughton, C.A., 1995, "Measurement of wind-induced heat transfer through permeable cold-weather clothing", Cold Regions Science Technology, **23**, pp. 305-316.

[3] – Patankar, S.V., 1980, "Numerical heat transfer and fluid flow", Hemisphere, New York, USA.

[4] – Casey, M., Wintergerste, T., 2000, "Quality and trust in Industrial CFD", ERCOFTAC-Sulzer Innotec, Winterthur Switzerland.

[5] – Fluent Incorporated, 1998, Fluent 5 User's Guide, Lebanon, USA.

[6] – Ferziger, J.H., Peric, M., 1996, "Computational Methods for Fluid Dynamics", Springer, Berlin, Germany.

[7] – White, F.M., 1991, "Viscous Fluid Flow", McGraw-Hill, Inc, New York, USA.

[8] – Fan, J., 1998, "Heat transfer through clothing assemblies in windy conditions", Textile Asia.

[9] – Zdravkovich, M.M., 1997, "Flow around circular cylinders", Oxford University Press, Oxford, UK.